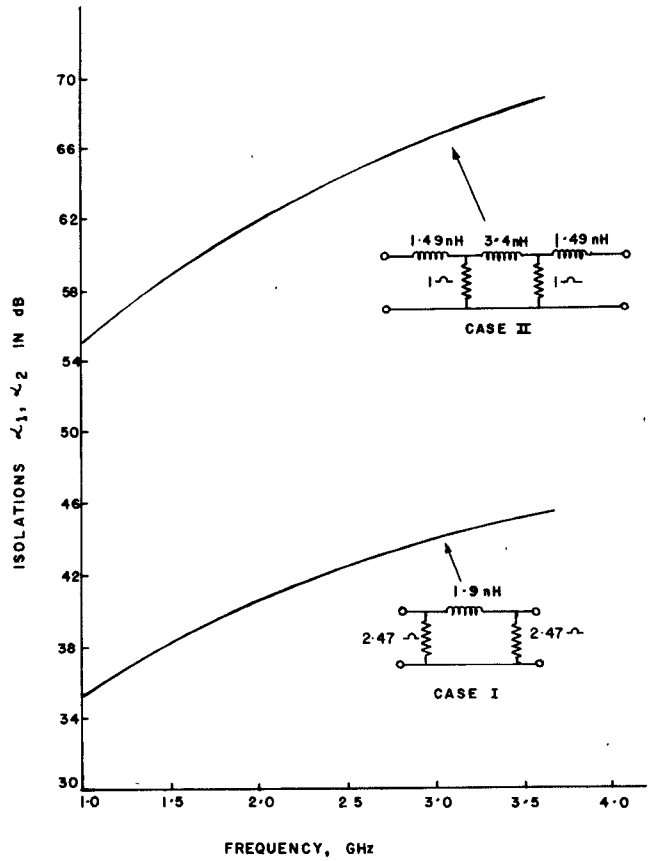

Fig. 2. Isolation versus frequency for passband VSWR = 1.05, f_{co} = 3.3 GHz, the resistances of the diodes when forward biased (or at high power) for case I and case II, are 2.47 and 1.0 Ω, respectively.

each and one series inductance of 1.9 nH, realized by a short coaxial high-impedance line length.

At forward bias or at high power level, the capacitances C_1 and C_3 will be replaced by the resistances of the diodes. Let us assume that the resistance of each diode is 2.47 Ω. The isolation of the switch/limiter is calculated using ***ABCD*** matrices [4] and is given by

$$\alpha_1 = 10\log\left[451.26 + 2902f^2\right]\text{dB} \tag{1}$$

where f is the frequency in GHz.

α_1 is plotted against frequency as shown in Fig. 2

Case II: Inductance as the First Element (Fig. 2)

For the same specifications as in case I, the low-pass filter elements values are $g_1 = 0.6181$, $g_2 = 1.2026$, $g_3 = 1.4130$, $g_4 = 1.2026$, and $g_5 = 0.6181$. Therefore,

$$L_1 = L_5 = \frac{g_1 Z_0}{2\pi f_{co}} = 1.49\text{ nH}$$

$$C_2 = C_4 = \frac{g_2}{2\pi f_{co} Z_0} = 1.16\text{ pF}$$

$$L_3 = \frac{g_3 Z_0}{2\pi f_{co}} = 3.4\text{ nH}.$$

Therefore, the required switch/limiter with passband VSWR of 1.05 will consist of two diodes with capacitances of 1.16 pF each and three series inductances (1.49 nH at the input, 3.4 nH in between the diodes, and 1.49 nH at the output) realized by short coaxial high-impedance line lengths.

At forward bias or high power level, the capacitances C_2 and C_4 are replaced by diode resistances. In order to compare the merits of the circuits in cases I and II, we have to take p-i-n diodes of the same cutoff frequency f_c. Assuming the same value for reverse- and forward-biased series resistances, we have $f_c = 1/2\pi C_1 R_1 = 1/2\pi C_2 R_2$. Therefore, $R_2 = (C_1/C_2)R_1 \cong 1.0$ Ω. Where R_1 (= 2.47 Ω) and R_2 are the forward-biased series resistances of each diode in case I and case II, respectively. The isolation α_2 is calculated using ***ABCD*** matrices and is given by

$$\alpha_2 = 10\log\left[\left(51 - 205.75f^2\right)^2 + 39.5f^2\left(91.44 - 2.98f^2\right)^2\right]\text{dB} \tag{2}$$

where f is the frequency in GHz.

α_2 is plotted against frequency as shown in Fig. 2.

III. Discussions and Conclusion

It is seen from Fig. 2 that the isolation is always greater (20 dB, approximately) in case II compared to case I, though the pass-band characteristic (with zero- or reverse-biased diode in the case of the switch and at low power level in the case of the limiter) is the same for both the cases. Therefore, a switch/limiter design based on the low-pass filter structure with series inductance as the first element will always offer higher isolation at the same time with low insertion loss.

References

[1] R. H. Brunton, "Switch high power with diodes," *Electronic Design*, Jan. 4, 1966.

[2] R. Garver, *Microwave Diode Control Devices*. USA: Artech House, Inc., 1976, pp. 157–160, pp. 333–349.

[3] G. L. Matthaei, Leo Young and E. M. T. Jones, *Microwave Filters, Impedance-Matching Networks and Coupling Structures*. New York: McGraw-Hill, 1964, pp. 86–102.

[4] J. F. White, *Semiconductor Control*. USA: Artech House, Inc., 1977, pp. 186–190.

On the Possible Use of Microwave-Active Imaging for Remote Thermal Sensing

J. C. BOLOMEY, L. JOFRE, AND G. PERONNET

Abstract **— Recent results have demonstrated the feasibility of quasi-real-time, active as well as harmless microwave imaging for biomedical purposes. Such a process allows tomographic reconstructions based on differences in the complex permittivity of tissues, the temperature dependence of which can be used for remote thermal sensing. A basic experiment conducted in water at 3-GHz yielded information on spatial resolution and temperature sensitivity. Discussion is devoted to potential capabilities and limitations of this remote-sensing approach in more complicated situations.**

Manuscript received January 18, 1983; revised May 3, 1983. This work was supported in collaboration with the Société d'Etude du Radant (Orsay) and the Laboratoire de Thermologie Biomédicale (Strasbourg) in the frame of a Délégation Générale pour la Recherche Scientifique et Technique under Contract 81M0909.

J. C. Bolomey and G. Peronnet are with the Groupe d'Electromagnetisme, Laboratoire des Signaux et Systèmes, Ecole Supérieure d'Electricite, Plateau du Moulon-91190 GIF-sur-Yvette, France.

L. Jofre is with the Departmento Electrotisica, Escuela Tecnica Superior de Ingenieros de Telecommunicación, Apdo. 3002 Barcelona-34, Spain.

0018-9480/83/0900-0777$01.00 ©1983 IEEE

I. Introduction

Difficulties of remote temperature sensing seriously limit the efficiency of heating processes involving, for example, microwaves. This limitation is particularly significant in biomedical hyperthermia. The most common procedure consists of measuring the temperature inside the region of interest by means of a more-or-less interfering sensor (by thermocouples or thermistors) [1]. In addition, such an invasive procedure only allows measurements at a finite number of points.

More recently, microwave thermography [2]–[4] has been successfully used to control hyperthermia in the clinic. This approach is strictly non-invasive but it suffers, at least until now, from two main limitations. First, only superficial temperatures are measured, and their translation in terms of subcutaneous temperature gradients is not an easy task [5], [6]. The difficulty mainly results from the largely uncontrolled extent of the domain under investigation. Some recent advances in the technique of correlative thermography tend to reduce this difficulty [7]. Second, due to its passive aspect (endogenous emissions), microwave thermography has poor sensitivity. Consequently, the rate of measurements is approximately one point per second. This low sampling rate is incompatible with efficient real-time imaging, even when multiple-probe arrays are used. Nevertheless, microwave thermography does present an advantage; it can provide calibrated temperatures with a resolution of a few tenths-of-a-Celsius degree.

Some recent experiments have demonstrated the feasibility of active microwave imaging of biomedical media [8]–[11]. Low irradiance levels, less than 1 mW/cm2, guarantee safe exposures. Furthermore, actual technologies allow quasi-real-time acquisition of data as well as numerical reconstructions. The images obtained by active microwave imaging tomographic projections are directly related to the local complex permittivity of the observed tissues. This complex permittivity is temperature dependent [12] in such a way that the images can be interpreted, from a more or less straightforward manner in terms of temperature differentials. This paper is devoted to the discussion of this particular use of active microwave imaging. In the first part, one establishes what can be seen in such images in terms of their implicit temperature content. In the second part, one describes an experiment conducted in water at 3 GHz. This experiment illustrates temperature sensitivity as well as the spatial resolution, and demonstrates the feasibility of remote temperature sensing. The term "sensing" indicates that the images need some interpretation in order to yield temperature measurements. Finally, the last part is devoted to a discussion of the limitations of the imaging process.

II. Microwave Tomography Processes

Until now, active microwave tomography has been developed in two main ways. The first approach is closely related to X-ray scanning and is based on a linear-path assumption of the rays between emitter and receiver. This transmission tomography (Fig. 1) provides measures of complex permittivity of tissues, which is akin to the use of X-rays to provide measures of density of tissues. Practically, the accuracy of the above-mentioned technique is improved by use of frequency-modulated equipments which allow selection of the most direct path between emitter and receiver.

The second approach, diffraction tomography, is more closely related to optical techniques. Conceptually, this kind of tomography could be achieved by means of a focusing system characterized by small field depth in such a way that the object is imaged, slice by slice. From a practical point of view, this task is better done by numerical processing of recorded holograms (Fig. 2). The result is the reconstruction of the equivalent currents, which are nothing more than the equivalent sources from which the object is viewed. At a point P, the equivalent current $\boldsymbol{J}(P)$ depends not only on the local complex permittivity $\epsilon_c(P)$ but also on the total field $\boldsymbol{E}_t(P)$ at that point

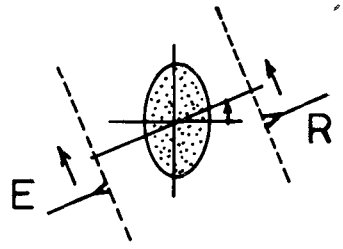

Fig. 1. Typical experimental arrangement for transmission tomography (See [8]). Emitting and receiving antennas are moved simultaneously. Projections are recorded for several aspect angles of the object under test.

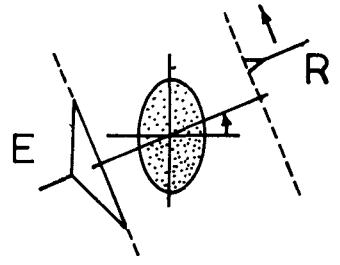

Fig. 2. Typical experimental arrangement for diffraction tomography (See [7]). Holograms are recorded by moving the receiving antenna. The process is iterated for several aspect angles of the object under test.

$$\boldsymbol{J}(P) = j\omega[\epsilon_c(P) - \tilde{\epsilon}]\boldsymbol{E}_t(P)$$

where ω is the angular frequency and $\tilde{\epsilon}$ is the permittivity of the reference medium, that surrounds the object under investigation. The total field is the superposition of the incident field $\boldsymbol{E}_i(P)$—the field that would exist in the absence of object and that is assumed to be known—and of the field $\boldsymbol{E}_S(P)$ scattered by the object which results from the radiation of the equivalent sources [13]

$$\boldsymbol{E}_t(P) = \boldsymbol{E}_i(P) + \boldsymbol{E}_S(P)$$

$$\boldsymbol{E}_S(P) = \frac{1}{j\omega\tilde{\epsilon}}[-\tilde{\gamma}^2 + \text{grad div}]\iiint_{\mathscr{D}} \boldsymbol{J}(P')\frac{e^{-\tilde{\gamma}|PP'|}}{4\pi|PP'|}d^3P'$$

where $\tilde{\gamma}^2 = -\omega^2\tilde{\epsilon}\mu$ is the propagation constant in the reference medium and $\mathscr{D}$ the domain occupied by the object. It appears that the previous equation provides the total field at any locus so far as $\boldsymbol{J}$ is known. The simultaneous knowledge of $\boldsymbol{J}$ and $\boldsymbol{E}_t$ allows one to determine the local permittivity constant $\epsilon_c(P)$. For near-homogeneous media, according to Born's approximation, the scatterered field can be neglected in the calculation of the equivalent currents in such a way that local permittivity can be directly derived from the equivalent current.

Microwave images realized by transmission or diffraction tomography can be closely related to local complex permittivity. Coming back to the considered problem, it is now worth noting that the complex permittivity is temperature dependent and is dependent as well on other physical factors (e.g., pressure and humidity). Such dependencies have been used in the past in various local sensing devices in the microwave and ultrasonic

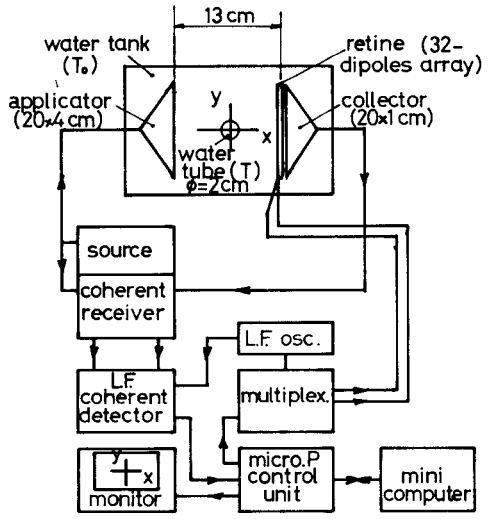

Fig. 3. Schematic view of the 3-GHz experimental setup.

domains. The question we address is to determine how the implicit temperature content of microwave images can be extracted in the stead of remote thermal sensing.

III. A Basic Experiment

Fig. 3 illustrates a simple two-dimensional problem. The body under investigation is a thin plastic tube filled with water at temperature T immersed in a water tank at temperature T_0. The tube's diameter is 2 cm, its thickness 0.2 mm. The use of a water medium was didacted by its similarities to tissues such as muscle with respect to their dielectric properties.

The measurement setup has been described in detail elsewhere [9]. Quasi-plane-wave illumination is produced by a horn applicator. The field probing over a line is achieved by means of the modulated scattering technique. An array of 32 diode-loaded dipoles is located in the aperture of a collecting horn. Modulation of the diodes in succession results in a signal at the output of this horn. The obtained signal is proportionnal to the field at the different dipole locations. The distance between two dipoles is one-half a wavelength in water (i.e., 6 mm at 3 GHz). By such a technique, measurement rates as high as 1000 points per second have been obtained. The distance between the applicator and the collector is 13 cm.

A numerical process based on a spectral domain approach [14] allows cross-sectional reconstruction of the media lying between the applicator and the probing line. Combining the measurements obtained by rotating the object under investigation has proved to provide a spatial resolution of approximately one-half a wavelength (in water). In the case of a circular tube, such a combination can be simulated from a single measurement because of its symmetry.

The experiment simply consisted of imaging the medium between the applicator and the collecting horn as the temperature T of water in the tube was changed. The water in the tank was fixed at $T_0 = 25°C$, and T was increased from 25 to 45°C. In order to improve the dynamic range, difference images have been displayed, with reference to the $T = 25°C$ case (Fig. 4). This is the reason why the corresponding image presents a black background. The images are relative to the modulus of the equivalent currents. They exhibit bright spots, the position of which correspond to the tube's location. The brightness variations of the spot are approximately linear with increasing temperature (Fig. 5). Such a dependence has been checked by measuring permittivity changes of the real and imaginary parts of the complex permittivity of water (Fig. 6) and by calculating the corresponding variations of the equivalent current under Born's approximation. Observed and predicted results agree quite well.

In this simple experiment, active microwave imaging provided a non-invasive mean for calibrated temperature change measurement with a spatial resolution of 6 mm through a thickness as large as a tenth of a centimeter. The temperature resolution is less than 1°C. This success results from the simplicity of the considered configuration. The next section is devoted to the applicability of this technique to more realistic situations.

IV. Discussion

For an arbitrary configuration, the interpretation of a microwave image in terms of temperature will be more difficult. First, the temperature sensitivity of the permittivity changes is intimately related to the molecular structure of the materials. It changes from one material to another. Even in a given material, sensitivity will change with frequency. Second, the limited spatial resolution introduces some integration of local permittivity gradients.

For these reasons, a complete remote-temperature-sensing test must consider:

1) recognition of the different constituents of the region under interest (such a recognition could be achieved from *a priori* anatomical knowledge and/or from X-ray scanning);
2) determination of the permittivity temperature dependence of the constituents (such a determination could result from systematic *in vivo* measurements and possible deviations from one patient to another must be taken into account); and
3) reconstruction of "difference" images during the imaging process, and correlative translation in terms of temperature with possible checks on local absolute values taken through classical means in the tested area.

If such a complete temperature testing is difficult to conceive in the contemporary biomedical domain, it might be realized in the near future if successful efforts are made with respect to point 2. Actually, only limited results are available for the temperature sensitivity of the permittivity of living tissues. But measurements made on excised tissues, fat or muscle, have already shown relative sensitivities of the same order as those for water [15]. In any event, this testing could be used in the domain of industrial application where materials are easier to characterize.

In spite of these difficulties, the suggested remote-temperature-sensing procedure presents some interesting features that result from:

1) the possibility of quasi-real time imaging of large areas with reasonable spatial resolution;
2) a total by harmlessness and non-invasive test that is compatible with continuous monitoring; and
3) a relative ease in handling and integration of heating electrodes and applicators (indeed, three-dimensional probing could be achieved by means of cross-linear arrays that minimize the number and spatial extent of the probes [16], [17] and such an array will be described in another paper).

These advantages make that active microwave imaging should compete significantly with other approaches to non-invasive ther-

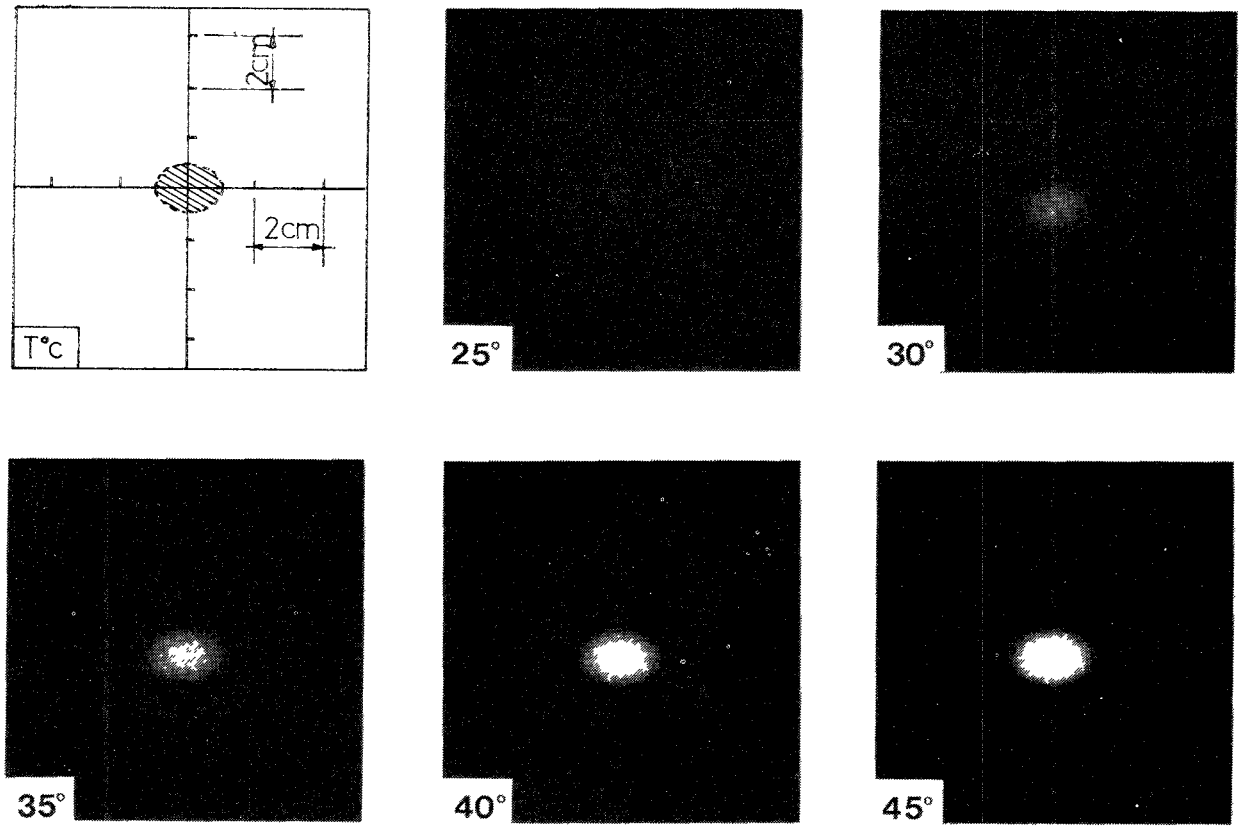

Fig 4. Tomographic views of the medium lying between applicator and collector for different temperature T

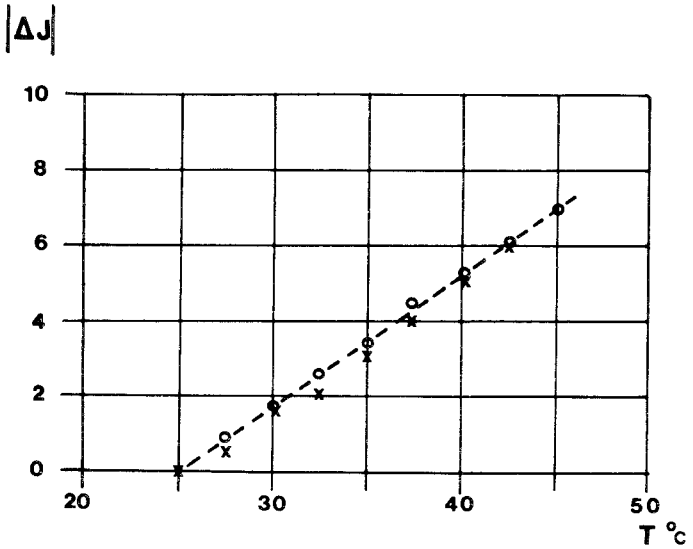

Fig. 5. Sensitivity of the spot brightness as a function of temperature T.

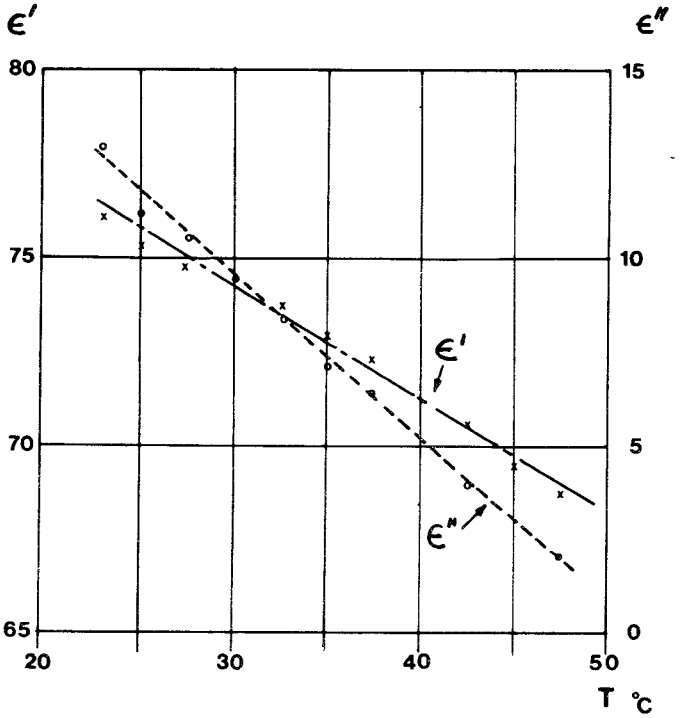

Fig. 6 Measured relative complex permittivity of water versus temperature $\epsilon_r = \epsilon' + j\epsilon''$

mometry such as thermography, ultrasonic echotomography [18], [19], and X-ray tomodensitometry [20].

References

[1] R. R. Bowman, "A probe for measuring temperature in RF-heated material," *IEEE Trans Microwave Theory Tech.*, vol 24, p. 43, Jan. 1976.

[2] M. Chive, M. Plancot, Y. Leroy, G. Giaux, and B. Prevost, "Progress in microwave and radiofrequency and hyperthermia controlled by microwave thermography," in *Proc. 3th. Int. Cong. Thermology*, Bath, England, Apr. 1982.

[3] Y. Leroy, "Microwave thermography for biomedical applications," in *Proc. 12th European Microwave Conf., Workshop Med. Appl.*, Helsinki, Finland, Sept. 1982.

[4] A. H Barret, P. C. Myers, and N. L Sadowsky, "Detection of breast cancer by microwave radiometry," *Radio Sci.*, vol 12, pp 167–171, 1977

[5] P Edenhofer, "Electromagnetic remote sensing of the temperature profile in a stratified medium of biological tissues by stochastic inversion of radiometric data," *Radio Sci* , vol. 16, pp. 1067–1069, 1981.

[6] B. Djermakoye and J. A. Kong, "Radiative-transfer theory for the remote sensing of layered random media," *J. Appl. Phys.*, vol. 50, pp. 6600–6604, 1979.
[7] A. Mamouni, Y. Leroy, J. C. Vand De Velde, and L. Bellarbi, "Introduction to correlation microwave thermography," in *Proc. 12th European Microwave Conf.*, Helsinki, Finland, Sept. 1982.
[8] J. H. Jacobi, L. E. Larsen, "Microwave time delay spectroscopic imagery of isolated canine kidney," *Med. Phys.*, vol. 7, pp. 1–7, 1980.
[9] J. C. Bolomey, A. Izadneghadar, L. Jofre, C. Pichot, G. Peronnet, and M. Solaimani, "Microwave diffraction tomography for biomedical application," *IEEE Trans. Microwave Theory Tech.*, Nov. 1982.
[10] H. Ermert, F. Fülle, and D. Hiller, "Microwave computerized tomography," in *Proc. 11th European Microwave Conf.*, Amsterdam, The Netherlands, 1981, pp. 421–426.
[11] S. Rao, K. Santosh, and E. C. Cregg, "Computed tomography with microwaves," *Radiology*, vol. 135, pp. 769–780, 1980.
[12] A. R. Von Hippel, *Dielectrics and Their Applications*. New York: Wiley, 1964.
[13] D. S. Jones, *Theory of Electromagnetism*. New York: Pergamon, 1964, ch. 6, p. 335.
[14] C. Pichot, L. Jofre, G. Peronnet, A. Izadnegahdar, and J. C. Bolomey, "An angular spectrum method for inhomogeneous bodies reconstruction," in *Proc. IEEE-AP/S Symp.*, Albuquerque, NM, May 24–28, 1982, pp. 664–667.
[15] J. L. Guerquin-Kern, "Hyperthermie locale par microondes en thérapeutique cancérologique," *Thèse*, Strasbourg, 20 Jun. 1980.
[16] S. Al Adhami, A. P. Anderson, and J. C. Bennet, "A novel radar array and its imaging properties," *IEEE Trans. Antennas Propagat.*, vol AP-27, no. 4, pp 567–570, 1979.
[17] M. Melek and A. P. Anderson, "Theoretical studies of localised tumour using focused microwave arrays," *IEE Proc.*, vol. 127, pt F, no. 4, Aug. 1980, pp. 319–321.
[18] J. Robert, C. Marchal, J. M. Escanye, P. Thouvenot, M. L. Gaulard, and A. Tosser, "Utilisation de la vélocimétrie ultrasonore pour le contrôle de l'hyperthermie," in *Proc. Int. Symp. Biomédical Thermology*, Strasbourg, Jul. 1981, p. E–73.
[19] R. Maini, M. F. Iskander, C. H. Durney, and M. Berggren, "On the sensitivity and the resolution of microwave imaging using ART," *Proc. IEEE*, vol. 69, no. 11, Nov. 1981, pp. 1517–1519.
[20] B. G. Fallone, P. R. Moran, and E. B. Podgorsak, "Non invasive thermometry with a clinical X-ray CT scanner," *Med. Phys.*, vol. 9, no. 5, pp. 715–721, Sept.–Oct. 1982.

On the Transient Analysis of Circuits Containing Multiple Diodes

P. A. BLAKEY AND R. K. FROELICH

Abstract — **Multiple-diode circuits are increasingly being used for power combining at microwave frequencies. This paper presents a method for the transient analysis of such circuits. The method exploits the cold-capacitance–particle-current decomposition of semiconductor diodes and is simpler, more efficient, and more accurate than previously proposed approaches to the problem.**

I. Introduction

Hiraoka [1] recently considered the problem of transient analysis of multiple nonequivalent transit-time diodes embedded in a circuit. This is a problem of considerable practical importance, especially in the area of power combining. The method demonstrated by Hiraoka combines the finite-difference equations associated with time-domain device simulation, together with the circuit equations, into a single matrix equation for the whole system. The implementation is inherently implicit and requires the inversion of a large matrix at each time step. The coefficients of the matrix to be inverted are time dependent and must be evaluated at each time step. Repeated inversion of a large matrix makes the method extremely expensive. The cost also increases much faster than linearly with the number of devices considered.

The purpose of this note is to present an alternative procedure which is simpler, more efficient, at least as accurate, and for which the cost increases only linearly with the number of devices considered.

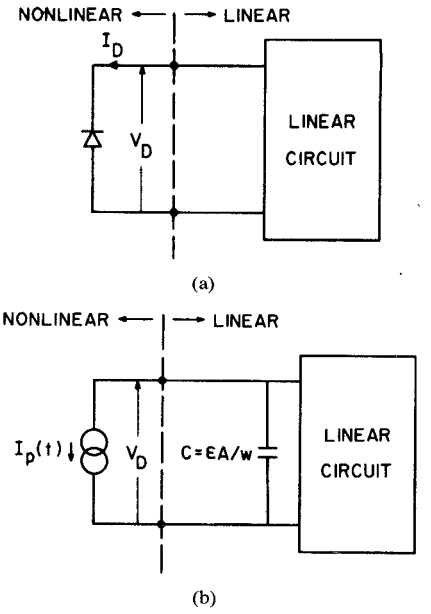

Fig 1. The diode-circuit partitioning. (a) Before the capacitance–particle-current decomposition. (b) After the capacitance–particle-current decomposition. $\{I_p(t) = (1/w)\int_0^w [I_e(x,t) + I_h(x,t)]\,dx\}$.

II. Alternative Methods

Most previous work has partitioned the system into a linear (circuit) part and a nonlinear (diode) part as in Fig. 1(a). The circuit part is treated using the well-established methods of linear system theory, and the diode part is treated using time-domain simulation. The time-domain simulation can be implicit or explicit. Different methods of linear system theory lead to different implementations. Evans and Scharfetter [2] used an impulse response/convolution integral approach with the convolution implemented using an FFT. Brazil and Scanlan [3] used state-space methods. Efficient procedures for handling mixed lumped-distributed circuits were developed by Mains *et al.* [4]. Care must be taken with the interfacing. An iterative procedure, involving at least two diode solutions, is generally adopted to obtain reasonable self-consistency between diode and circuit current and voltage. Avoidance of this iteration is a major motivation of Hiraoka's approach.

Blakey *et al.* [5] used the same device–circuit partitioning with an explicit diode/circuit interaction. This method is efficient but not very general; the circuit element next to the diode has to be an inductance, and for small enough values of inductance the accuracy of the method can be unacceptably low.

III. An Accurate and Efficient Explicit Method

The authors' present method involves a modification of the diode/circuit partitioning. The cold-capacitance–particle-current generator decomposition (see Appendix I) is performed for the

Manuscript received January 26, 1983; revised May 2, 1983. This work was supported by Air Force Avionics Laboratory, Wright-Patterson Air Force Base, OH.

P. A. Blakey is with the Electron Physics Laboratory, Department of Electrical and Computer Engineering, University of Michigan, Ann Arbor, MI 48109.
R. K. Froelich is with Watkins Johnson Co., Palo Alto, CA.

0018-9480/83/0900-0781$01.00 ©1983 IEEE